A new insight on the understanding of carbonisation and graphitisation mechanisms

Pascal Puech, Marc Monthioux

A new insight on the understanding of carbonisation and graphitisation mechanisms

Pascal Puech[*], Marc Monthioux[*]

Centre d'Elaboration des Matériaux et d'Etudes Structurales (CEMES), UPR-8011 CNRS, Université de Toulouse, France.

I. Introduction

During primary and secondary carbonisation and then graphitisation processes, any organic precursor is subjected to structural changes which make it evolve from isotropic to anisotropic, in an extent related to the starting elemental composition, and then to the graphitisability. Transmission electron microscopy studies[1] have confirmed that all the crystallites within a graphenic material are somewhat similar in size for a given ''maturity'' (that is to say, the level of structural evolution as reached by the joint effect of temperature and time). This is very convenient because it means that any graphenic material can be represented by a single average crystallite, which dimensions L_a (in-plane) and L_c (perpendicular to the planes) are supposedly accessible by X-ray diffraction. Therefore, for decades, analysing X-ray diffraction (XRD) patterns was used to evidence the related structural evolution of the material, aiming at extracting the average crystallite dimensions L_a and L_c as they closely relate to the material properties (i.e., mechanical, thermal, and electrical). However, in particular because of the two-dimensional nature of the graphene-based crystallites which develop in the material and, upon heat-treatment, either remain so for non-graphitisable carbons or gradually convert partially or fully into three-dimensional crystals for graphitizable carbons, accurately analysing XRD patterns has been an issue for the last 80 years[2-6]. Indeed, the turbostratic structure induces distortion in some of the diffraction peaks which make that fitting them and extracting the crystallite dimensions (more specifically L_a) is not straightforward. Almost all the attempts to address this issue were and still are based on trying to fit experimental XRD patterns with mathematical

---
[*] Corresponding authors: <pascal.puech@cemes.fr>; <marc.monthioux@cemes.fr>

functions[6-19], which some are poorly accounting for the physical, structural reality. Such an approach may be designated as a top-down approach. In opposition to this standard route, and based on what is known about the carbonisation mechanisms as published in the long-time-documented literature[20-23], we propose a bottom-up approach for analysing XRD data which is unprecedented but in a pioneering attempt by Fujimoto[24]. The resulting new fitting procedure was tested on two material series (a coal-tar pitch coke series, and an anisotropic 1050°C-pyrolytic carbon series) annealed over a large temperature range, from 1000 to 2650°C. Only results on the coke series are reported here. Results on the pyrolytic carbon series were reported in ref[25] along with a more detailed description and discussion of the methodology and of the results on the coke series.

II. Fitting methodology and results

Supported by a close examination of the literature dealing with the carbonisation-graphitization processes back to Franklin, Maire, Méring, and others[20-23], our approach is based on 3 principles:

(i) In the course of the material structuration, randomly stacked AB pairs form, in addition to genuine turbostratic, and genuine graphitic (Bernal ABA, ABAB, etc.) stacking configurations. Randomly (= turbostratically) stacked AB pairs, randomly (= turbostratically) stacked single graphene, and "graphetically" stacked graphenes (3 or more) are the only three possible Basic Structural Components (BSCs) as illustrated in Figure 1.

(ii) graphene pairs (or triplets, quadruplets, etc.) within the same $00l$-coherent stack can exhibit different stacking sequences (i.e., turbostratic or graphitic) whatever the number of graphenes in the stack, instead of considering a coherent stack as a whole in which the constituting graphenes are stacked the same way. Turbostratically stacked single graphenes, AB pairs, and graphitic sub-domains are then able to co-exist within the same average crystallite of height L_c, therefore sharing the same L_a.

(iii) switching from turbostratic to graphitic stacking does not occur at the same time for all the graphene pairs within a same $00l$-coherent stack, as it depends on local steric constrains and on the type of defects peripheral to each of the graphenes.
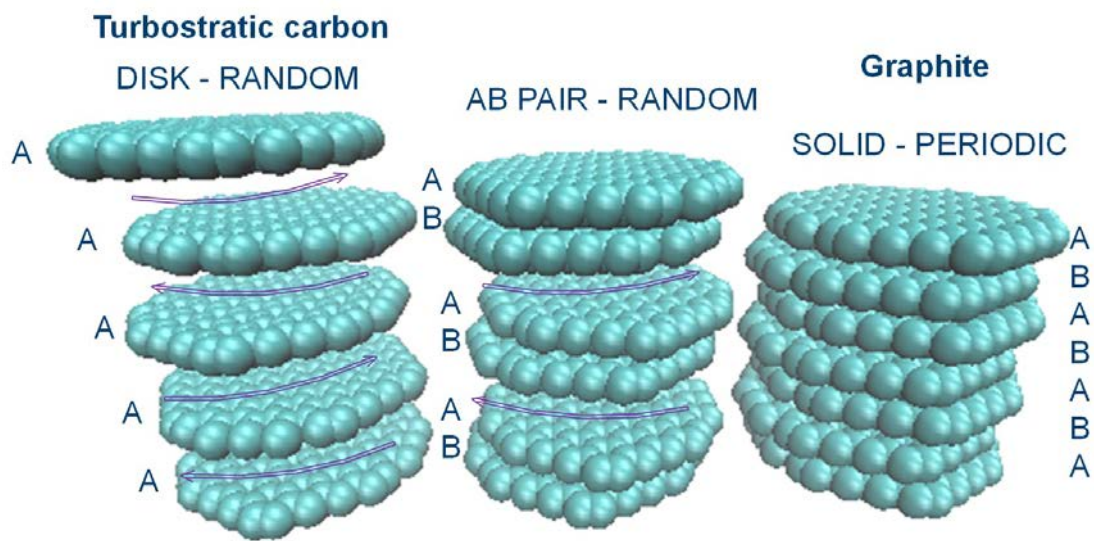
Figure 1: *Sketches of the modelled average* 00l*-coherent graphene crystallite for 100% turbostratic (left), 100% AB pairs (middle), and 100% Bernal stacking (right), so-called Basic Structural Components. All of them may eventually mix within the same average crystallite, hence they share the same* L_a *size.*

Discriminating between turbostratic and graphitic stacking sequences implies an intergraphene distance of 0.344 and 0.335 nm, respectively, as the only two possible intergraphene distances in the material. However, this is a simplification, because it is known that the intergraphene distance in immature graphenic carbons (such as low-temperature cokes, or kerogens) can exceed 0.344 nm by far, up to 0.6 nm and more[26].

Our bottom-up fitting methodology accounts for the above three principles by considering the optimized proportions of each BSC in the experimental pattern profiles, thanks to atomistic modelling of crystallite of various dimensions, the subsequent calculation of the related XRD profiles for each BSC, and then the parametrization of the BSC contribution (Figure 2). From Figure 2, some surprising features of the calculated XRD pattern of the AB pair BSC are noteworthy. One is that its *10* band profile is even more asymmetric than that of the purely turbostratic configuration. Another is that its *11* band exhibits a very different profile from that of its *10* band, showing no asymmetry, as opposed to the *10* and *11* bands for the turbostratic BSC which show similar profiles. Therefore, it can be guessed that the AB pair BSC will be of significant contribution when fitting the

experimental spectra, as opposed to the standards approaches which only consider either the turbostratic or graphitic cases.

Our parametrization is then adapted to the actual experimental pattern profiles (bottom-up approach), instead of adapting the profiles to pre-determined mathematical functions, as was usually performed so far (top-down approach). This means that experimental XRD patterns are always accurately fitted with meaningful functions, i.e., which are generated by actual structuration events.
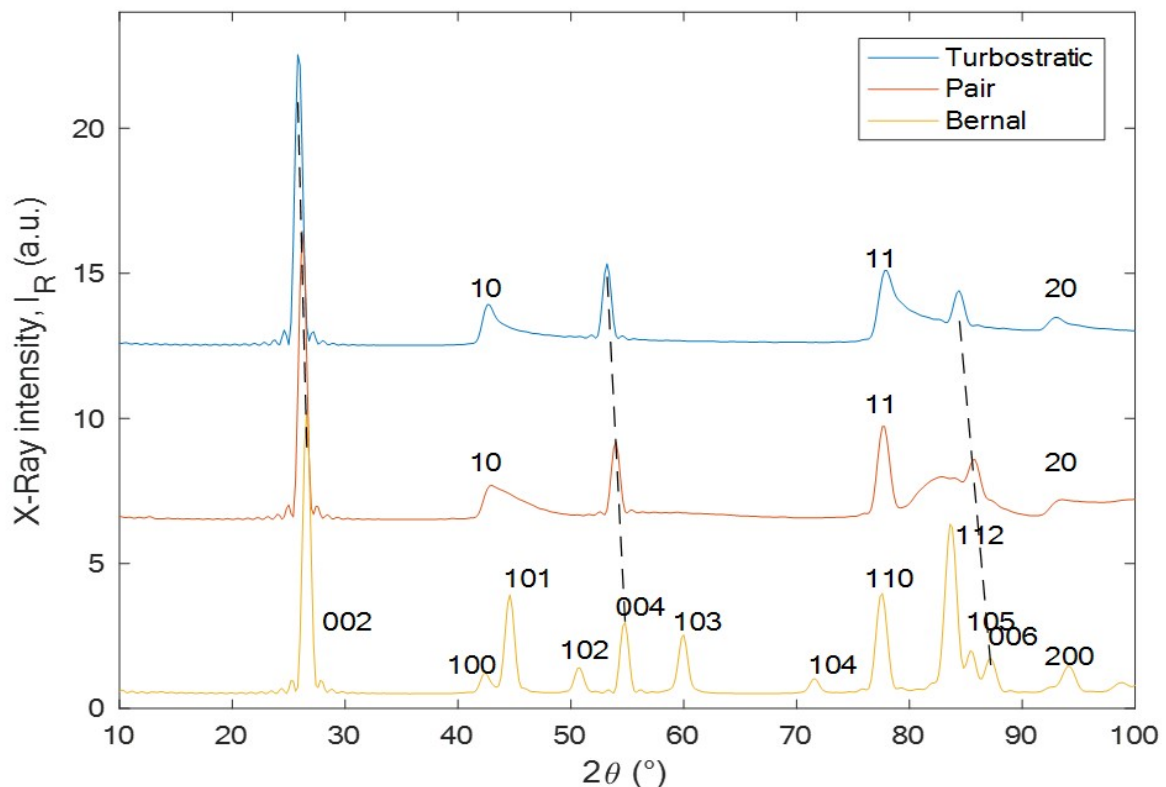

Figure 2: calculated XRD patterns for the turbostratic (top), AB pair (middle) and Bernal (bottom) BSC respectively, considering the example of a L_a size of 10 nm. The XRD pattern of a fully turbostratic carbon material will look like the top profile, that of a fully graphitic material will look like the bottom profile, and the profile for any carbon material with an intermediate structure state will exhibit a profile in-between while combining with a variable contribution of the middle profile (AB pairs).

Then, in order to fit any experimental pattern profile, the computer is first left free to find out an overall fitting function, whatever it is, and then to parametrize it. Afterwards, the

computer is again left free to fit at best this function by selecting the best proportions for the possible contributions of each of the BSCs. Therefore, the proportions of the latter are determined by the quality of the fit, eventually leading to discard one or two among the three BSCs. Importantly, the L_a value was left free to vary from a sample to another, but each of the contributing BSC within the same sample is given the same L_a. The possibility to vary slightly the C-C bond length (0.142 nm) was added to provide some flexibility and allow accounting for internal strains, also helping to converge but without significant influence to the final results (less than 1%).

The resulting fitting for all the spectra over the full carbonisation-graphitisation temperature range is perfect, or close to be[25]. An interesting consequence of this approach is that the proportion for each of the BSCs can be monitored all over the sample series (Figure 3). It can be seen that the material is 100% turbostratic first, and then suddenly (at 1650°C) starts being composed of turbostratically stacked single graphenes and AB pairs, and then is made of the three BSCs for a short temperature range (2050-2100°C) after which isolated graphenes disappear, and then the proportion of the Bernal stacking increases to the detriment of the AB pairs. Achieving such a fully meaningful evolution is remarkable because it was determined by the computer only by trying to fit the experimental spectra at best.
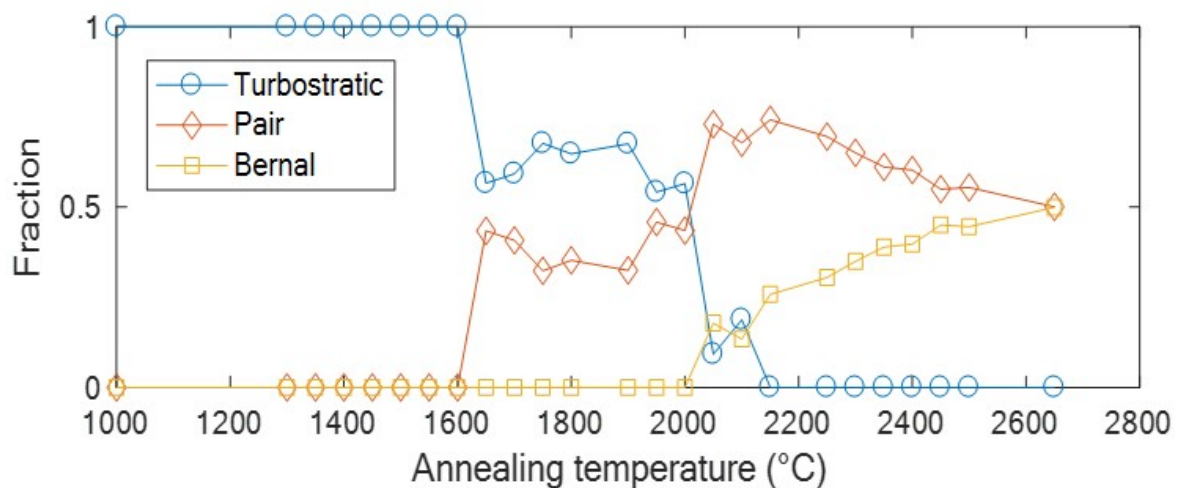

Figure 3: *Variation of the various BSC proportions with the annealing temperature for a coal tar pitch coke series. It appears that 2650°C is not enough for the graphitic order to fully develop.*

Another valuable consequence is the introduction of a new structural parameter L_c' (Figure 4), which is the height of the average genuine graphitic sub-domain contributing to the average crystallite of a carbon material in which graphitization has started but is not completed yet (or will never be, for a partially-graphitizable carbon). It can be calculated from the *101* or *112* peaks. Even at the ultimate temperature of the series where L_c reaches several tens of nanometres, the value of L_c' remains in the range of few nanometres[25], meaning that the average crystallite is far from having become a single graphite crystal yet. This is consistent with the known statement that genuine, bulk graphitisation requires temperatures as high as 3000°C[27].

From the calculated combination of the various BSCs, the evolution of the L_a value in the average crystallite all along the increasing annealing temperature can be obtained, as reported in Figure 4a. On the other hand, the evolution of L_c is also reported, yet obtained the regular way, i.e. by calculating them from the various *002* peaks thanks to the Scherrer equation (Figure 4b). It is remarkable that both exhibit a regime change in the range 2000-2100°C(corresponding to the long-time acknowledged carbonisation-graphitisation transition), whereas the respective calculation methods are totally different and independent.
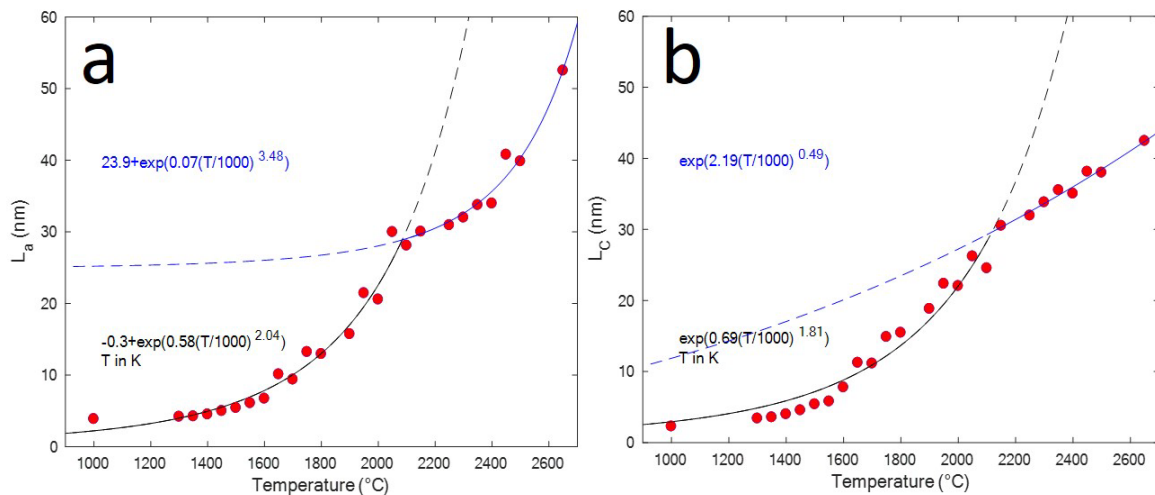

Figure 4: *(a) and (b) Plots of the* L_a *and* L_c *values respectively, versus the annealing temperature for the coal tar pitch-based coke series (corrected from the instrument line shape function).*

In addition to the consistency of the results such as that reported in Figures 3 and 4, various observations confirm the validity of our approach and methodology. One is to check whether fitting correctly a XRD spectrum in the transition zone (where the computer found that all the three BSCs should be present) is possible while ignoring the possible existence of AB pairs. This is reported in Figure 5 for the 2100°C-annealed coke. It is obvious that the only possibility to fit he experimental spectrum well is to consider the existence of the AB pairs in addition to the turbostratic and Bernal BSCs (Figure 5c).
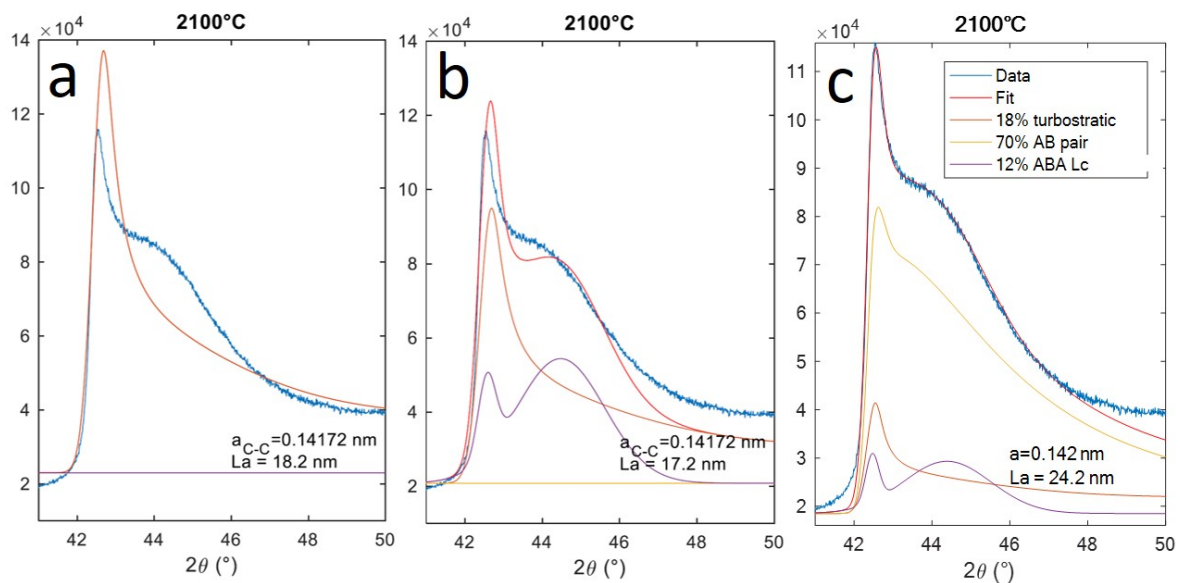

Figure 5: *The same XRD spectrum (2100°C-annealed coal tar pitch coke) in the* 10(0)-101 *region fitted by considering (a) the turbostratic BSC only; (b) the optimised combination of both the turbostratic and the Bernal BSCs, (c) the possible concomitant existence of the three BSCs (hence including the AB pairs). Blue line is the experimental spectrum. Red line is the fit. Other lines are the contributions of the various BSCs.*

Another validation is obtained when considering the plot of the d_{002} value versus the annealing temperature for both the values obtained from merely considering the Bragg law on the one hand, and from considering the respective contributions of the 0.344 and 0.335 nm intergraphene distances calculated from the BSC proportions provided by the model, on the other hand. This is reported in Figure 6. Because both calculation methods are totally independent, It is again remarkable that the two related plots follow exactly the same trend, and reveal d_{002} fluctuations (arrowed) for exactly the same samples. In addition to validating

our approach, this indicates that the d_{002} fluctuations arrowed are not due to some measurement uncertainty, but are real and intrinsic to the samples, for instance induced by a poor regulation of the temperature during the annealing step.
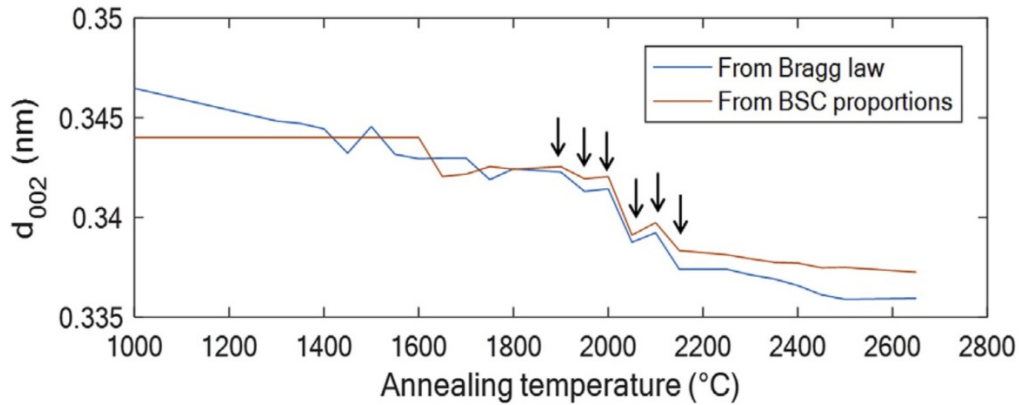

Figure 6: *Plot reporting the variation of the average* d_{002} *value along with the increasing annealing temperature for the coal tar pitch coke series. The blue line is obtained from considering the Bragg law and the angular variation of the 002 peak position from an experimental spectrum to another. The red line is obtained from calculating the* d_{002} *values resulting from the variable contributions of the 0.344 and 0.335 nm intergraphene distances corresponding to the BSC proportions for each temperature. The offset in the low temperature range is due to the fact that* d_{002} *values larger than 0.344 nm were not considered in the calculated model. The offset in the high temperature range is due to a slight overestimation of the AB pair proportion.*

Finally, a third validation of our approach is brought by comparing the L_a values calculated from the *10(0)-101* and the *11(0)-112* 2θ regions of the experimental spectra of various cokes of our sample series, using our methodology. The values are fully consistent (Figure 7), despite the contribution of the AB pairs in both 2θ regions are quite different (see Figure 2, middle).
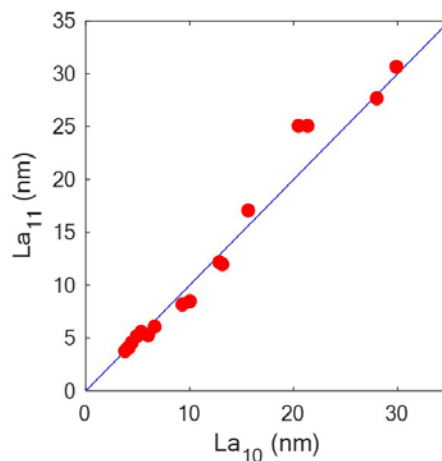
Figure 7: *Plot of the* La *values obtained for various coal tar pitch cokes annealed at increasing temperature, as calculated from either the* 11(0)-112 *or the* 10(0)-101 *regions of the experimental spectra. The blue line indicates the path of perfect equality.*

It worth noting that obtaining the same L_a values from the *100* and the *110* bands has always been an issue by using the regular, top-down approach, as an additional indication that the hypotheses on which it is based do not account for the whole physical meaning of the XRD spectra.

III. Conclusions

It is believed that this work (i) puts a new light on the structuration mechanisms of graphenic materials; (ii) provides a new procedure valid for a large range of graphenic materials which is able to give reliable values for key parameters such as L_a (the dimension of the average crystallite in the in-plane direction), a new parameter L_c' (the average dimension of the Bernal sub-stacks in the average crystallite, in the direction perpendicular to the basal plane), and the proportions of the various BSC contributions. On the other hand, because the *00l* peaks – and specifically the *002* peak - are not affected by the profile asymmetry generated by the occurrence of both the turbostratic and AB pair BSCs, the information which can be drawn from it (the average intergraphene distance d_{002}, the height dimension L_c of the average crystallite) may still be obtained by standard procedures (using the Bragg law and the Scherrer equation, respectively). By considering the L_a, L_c, L_c', d_{002}, and BSC proportion, which are now able to be reliably obtained, comparing carbon sample series

should be more accurate than ever. Improving the method is ongoing by refining the model on the one hand, and by considering new BSCs corresponding to the contribution of stacking faults (rhombohedral stacking) on the other hand.

Acknowledgments

References

1. Oberlin A, Carbon 22 (1984) 521-541.
2. Warren B E, *Phys Rev* 59 (1941) 693-698.
3. Bacon G E, *Acta Crystallogr* 4 (1951) 558-561.
4. Warren B E & Bodenstein P, *Acta Crystallogr* 20 (1966) 602-605.
5. Warren B E & Bodenstein P, *Acta Crystallogr* 18 (1965) 282-286.
6. Houska C R & Warren B E, *J Appl Phys* 25 (1954) 1503-1509.
7. Diamond R, *Acta Crystallogr* 11 (1958) 129-138.
8. Ruland W, *Acta Crystallogr* 18 (1965) 992-996.
9. Ergun S, in *Chemistry and Physics of Carbon vol. 3*, edited by Walker P L Jr (Marcel Dekker, New York), 1968, pp. 211-288.
10. Shiraishi M & Kobayashi K, *Bull Chem Soc Jpn* 46 (1973) 2575-2578.
11. Shi H, Reimers J N & Dahn J R, *J Appl Crystallogr* 26 (1993) 827-836.
12. Fujimoto H & Shiraishi M, *Carbon* 39 (2001) 1753-1761.
13. Ruland W & Smarsly B, *J Appl Crystallogr* 35 (2002) 624-633.
14. Iwashita N, Park C-R, Fujimoto H, Shiraishi M & Inagaki M, *Carbon* 42 (2004) 701-714.
15. Zickler G A, Smarsly B, Gierlinger N, Peterlik H & Paris O, *Carbon* 44 (2006) 3239-3246.
16. Li Z Q, Lu C J, Xia Z P, Zhou Y & Luo Z, *Carbon* 45 (2007) 1686-1695.
17. Loeh M O, Badaczewski F, Faber K, Hintner S, Bertino M F, Mueller P, Metz J & Smarsly B M, *Carbon* 109 (2016) 823-835.

18. Shi H, Reimers J N & Dahn J R, *J Appl Crystallogr* 26 (1993) 827-836.

19. Babu V S & Seehra M S, *Carbon* 34 (1996) 1259-1265.

20. Franklin R E, *Proc Roy Soc Lond A* 209 (1951) 196-218.

21. Franklin R E, *Acta Crystallogr* 4 (1951) 253-261.

22. Maire J & Méring J, in *Chemistry and Physics of Carbon vol. 6*, edited by Walker P L Jr (Marcel Dekker, New York), 1970, pp. 125-190.

23. Monthioux M, Oberlin M, Oberlin A, Bourrat X & Boulet R, *Carbon* 20 (1982) 167-176.

24. Fujimoto H, *Carbon* 41 (2003) 1585-1592.

25. Puech P, Dabrowska A, Ratel-Ramond N, Vignoles G L & Monthioux M, *Carbon* 147 (2019) 602-611.

26. Oberlin A, Boulmier J-L & Villey M, in *Kerogen*, edited by Durand B. (Technip, Paris), 1980, pp. 191-241.

27. Fischbach D B, in *Chemistry and Physics of Carbon vol. 7*, edited by Walker P L Jr (Marcel Dekker, New York), 1971, pp. 1-105.

Abstract

During carbonisation (primary and secondary) and then graphitisation processes, any organic precursor is subjected to deep structural changes which make it evolve from an isotropic to an anisotropic material, with the extent of the anisotropy being related to the starting elemental composition, and ultimately to the graphitisability. For decades, analysing X-ray diffraction patterns has been used to evidence the related structural evolution of the material, aiming at extracting the average crystallite dimension L_a and L_c as they closely relate to the material physical properties. In particular because of the two-dimensional nature of the graphene-based crystallites which develop in the material and, upon heat-treatment, either remain so for non-graphitisable carbons or gradually convert partially or fully into three-dimensional crystals for graphitizable carbons, accurately understanding and analysing XRD patterns has always been an issue. A new approach for analysing XRD data is described, designated as "bottom-up", meanwhile introducing the concept of Basic Structural Component. A better knowledge of the overall thermally-driven structure changes which occur in the material from the coke stage to the ultimate temperature of 2800°C is achieved, which is expected to apply to any kind of carbons, whatever their graphitisability.

Figure captions

Figure 1: Sketches of the modelled average 00l-coherent graphene crystallite for 100% turbostratic (left), 100% AB pairs (middle), and 100% Bernal stacking (right), so-called Basic Structural Components. All of them may eventually mix within the same average crystallite, hence they share the same L_a size.

Figure 2: calculated XRD patterns for the turbostratic (top), AB pair (middle) and Bernal (bottom) BSC respectively, considering the example of a L_a size of 10 nm. The XRD pattern of a fully turbostratic carbon material will look like the top profile, that of a fully graphitic material will look like the bottom profile, and the profile for any carbon material with an intermediate structure state will exhibit a profile in-between while combining with a variable contribution of the middle profile (AB pairs).

Figure 3: Variation of the various BSC proportions with the annealing temperature for a coal tar pitch coke series. It appears that 2650°C is not enough for the graphitic order to fully develop.

Figure 4: (a) and (b) Plots of the L_a and L_c values respectively, versus the annealing temperature for the coal tar pitch-based coke series (corrected from the instrument line shape function).

Figure 5: The same XRD spectrum (2100°C-annealed coal tar pitch coke) in the *10(0)-101* region fitted by considering (a) the turbostratic BSC only; (b) the optimised combination of both the turbostratic and the Bernal BSCs, (c) the possible concomitant existence of the three BSCs (hence including the AB pairs). Blue line is the experimental spectrum. Red line is the fit. Other lines are the contributions of the various BSCs.

Figure 6: Plot reporting the variation of the average d_{002} value along with the increasing annealing temperature for the coal tar pitch coke series. The blue line is obtained from considering the Bragg law and the angular variation of the *002* peak position from an

experimental spectrum to another. The red line is obtained from calculating the d_{002} values resulting from the variable contributions of the 0.344 and 0.335 nm intergraphene distances corresponding to the BSC proportions for each temperature. The offset in the low temperature range is due to the fact that d_{002} values larger than 0.344 nm were not considered in the calculated model. The offset in the high temperature range is due to a slight overestimation of the AB pair proportion.

Figure 7: Plot of the L_a values obtained for various coal tar pitch cokes annealed at increasing temperature, as calculated from either the *11(0)-112* or the *10(0)-101* regions of the experimental spectra. The blue line indicates the path of perfect equality.